Journal of Engineering Mathematics (2006) 54: 71–88
DOI 10.1007/s10665-005-9001-6


# Sloshing in a vertical circular cylindrical tank with an annular baffle. Part 1. Linear fundamental solutions

I. GAVRILYUK[1], I. LUKOVSKY[2], Yu. TROTSENKO[2] and A. TIMOKHA[3]
[1]*Berufakademie Thüringen-Staatliche Studienakademie, Am Wartenberg 2, 99817, Eisenach, Germany;* [2]*Institute of Mathematics, National Academy of Sciences of Ukraine, Tereschenkivska 3, 01601, Kiev, Ukraine;* [3]*Centre for Ships and Ocean Structures, Norwegian University of Science and Technology, 7491, Trondheim, Norway (E-mail: tim@imath.kiev.ua)*

Received 29 October 2004; accepted in revised form 24 May 2005

**Abstract.** The paper centres around fundamental solutions of the linearised problem on fluid sloshing in a vertical circular cylindrical tank having a thin rigid-ring horizontal baffle. It develops an analytically oriented approach, which provides accurate approximations of natural frequencies and modes. The singular asymptotic behaviour of the velocity potential at the sharp baffle edge is also captured. A numerical analysis quantifies the natural frequencies and modes versus vertical position and width of the annular baffle. Forthcoming parts will use these approximate fundamental solutions in both nonlinear modal modelling and estimating the damping due to vorticity stress near the baffle.

**Key words:** Galerkin's method, linear sloshing, natural frequencies, rigid baffle, transmission

## 1. Introduction

A fluid occupying partly either earth-fixed basins or moving tanks of rockets, nuclear reactors, tower- and bridge constructions, ships and liquefied natural gas carriers may perform wave motions relative to its hydrostatic equilibrium. These wave motions are called "sloshing".

Sloshing in mobile tanks is typically generated by guidance and control systems commands, manoeuvres and structural vibrations. It leads to severe hydrodynamic force- and moment loads on the tank walls. These are a danger for structural integrity and can produce a dramatic feedback sensed and responded to by the tank motions. The interaction-chain "control command – structural motions – sloshing – hydrodynamic loads – new control command" forms a closed loop, which may lead to instability and even damage. This occurs, for instance, when a structural frequency is close to a fundamental sloshing frequency. Since the lowest fundamental sloshing mode is characterised by the weakest damping, the design of slosh-suppressing devices should aim at shifting the lowest sloshing frequency away from the dominating structural frequency. By ensuring the splitting of these two effective frequency domains (sloshing and structural), installation of such a slosh-suppressing device guarantees the smallness of surface waves. As a consequence, sloshing can be described by a *linear theory*.

In view of minimising the crucial loads, preventing structural failure and governing the fluid position within the tank, extensive experimental and theoretical studies have been undertaken since several decades and, as a result, numerous devices have been designed for suppressing the fluid mobility. Systematisations of various slosh-suppressing devices have at different times and for different applications been carried out by Abramson [1], Bauer [2], Mikishev and Rabinovich [3], Mikishev and Churilov [4], Mikishev [5], Ibrahim *et al.* [6].

They formulated design criteria. In particular, the NASA design criteria [1] suggest either subdividing the container by longitudinal (vertical) walls [7,8] or installing baffles. As long as the compartment is characterised by increasing structural mass, baffling is almost always cheaper, without the weight penalty.

Sloshing in the so-called tuned liquid dampers (TLDs) can be used for mitigating the structural vibrations of large buildings, towers and bridges resulting from external impacts and earthquakes. Contrary to sloshing in mobile vehicles carrying fluids, this kind of application requires overlapping the primary sloshing and structural frequency domains. As a consequence, the coupled "structure-fluid" vibrations become strongly resonant and lead to large-amplitude surface waves. Since the total kinetic energy is then re-distributed in favor of the fluid mass, the amount of structural damping increases dramatically. Analysis of resonant sloshing in the baffled TLDs should therefore be based on a *fully nonlinear formulation*. This implies requirements for robust and accurate computer programs. Reviews of these are presented by Solaas [9], Cariou and Casella [10]. Some successful simulations of baffled fluid sloshing can be found in [11–15].

The nonlinear sloshing problem needs also analytically oriented methods that clarify the physical nature of resonant sloshing. The physical nature is quite different for distinct tanks' shapes and fluid fillings. As explained in the analytical and experimental works by Ockendon *et al.* [16], Faltinsen and Timokha [17], Yalla [18], resonant sloshing with small fluid depths is characterised by shallow-water phenomena including wave breaking, bores and overturning. These phenomena are caused by the nearly commensurate fundamental sloshing spectrum that leads, due to the nonlinearity, to progressive resonant activation of higher modes, which are responsible for short, steep surface waves. Since shallow flows are strongly dissipative, the total structural damping increases, even without installing slosh-suppressing devices. In contrast, sloshing in smooth tanks with a finite fluid depth resembles long free-standing waves. These are characterized by small damping rates [18–20] and, therefore, the corresponding TLDs need baffling to both decreased wave responses [15,21] and increased damping caused by vorticity forces at the sharp baffle edges. The latter has been the main focus of many investigators including Keulegan and Carpenter [22], Miles [23], Mikishev and Rabinovich [3], Mikishev [5], Sarpkaya and O'Keefe [24], and, recently, Buzhinskii [25], Isaacson and Premasiri [26]. They showed that, if wave magnitudes are relatively small, the vorticity-based damping can be quantified within the framework of a linear inviscid potential model. The appropriate hydrodynamic analysis introduces the so-called velocity intensity factor, the coefficient $K_v$, appearing at the main singular term of the velocity potential along the sharp baffle edge. By mentioning that an analogous problem arises in linear fracture mechanics (when calculating the stress-intensity factors at a sharp edge of a crack in a solid), Buzhinskii discussed the difficulties of quantifying $K_v$ by traditional Computational Fluid Dynamics methods. He called for new analytically oriented methods capturing the singular behaviour of the velocity potential.

The present paper presents results of an applied mathematical project on analytical approaches to fluid-sloshing problems in tanks with baffles. For brevity, the project restricts itself to relatively simple tanks (exemplified in this paper by a vertical circular cylinder) and involves three consequent, linked parts:

Part 1: Development of analytically oriented methods for the linearised fluid-sloshing problem that approximate the natural frequencies as precise as the singular asymptotics of the velocity potential.

Part 2: Generalisation of nonlinear modal methods for theoretical classification of steady-state resonant fluid motions in the manner of Lukovsky [27], Faltinsen *et al.* [19,28] and Gavrilyuk *et al.* [29] for smooth cylindrical tanks.

Part 3: Quantification of fluid damping due to vorticity stress at the baffle edge by utilising the Buzhinskii formula [25].

The linear sloshing in a circular cylindrical tank with rigid baffles has been studied by many authors in the context of spacecraft applications. Experimental and numerical results were reported by Dokuchaev [30], Bauer [2], Rabinovich [31], Ermakov *et al.* [32], Trotsenko [33], Morozov [34] and, recently, by Watson [35], Biswal *et al.* [36], Gedikli and Ergüven [37, 38]. Most of the computational results were based on finite-element schemes. These provide sufficient accuracy for computing some of the lower natural frequencies, but do not capture the singularity at the baffle edge. Besides, the approximate velocity potential does not admit higher derivatives.

To the authors' knowledge, there is a very limited set of analytically oriented approaches to the linear sloshing problem in baffled tanks. Examples are presented by Trotsenko [39,40], Galitsin and Trotsenko [41] and, for the problem of scattering by vertical barriers, by Porter and Evans [42]. After a detailed reading of these papers, we found it possible to develop similar approximate methods. As a result, a simple, efficient and precise *engineering* variational method was obtained. It guarantees six significant figures of the natural sloshing frequencies and five figures for the natural modes (in uniform metrics) with a small (up to 9) number of basic functions. The capabilities of the method are demonstrated by numerical examples. An analysis of the linear sloshing frequencies versus geometric size and vertical position of the baffle is also done. The method is invalid when either baffle is very close to the mean fluid surface or a baffle is sufficiently wide to prevent the flux between lower (under the baffle) and upper (over the baffle) fluid domains. Mathematical and physical explanations of these failures are given. In particular, decreasing the length between baffle and hydrostatic fluid plane leads to either slopping or shallowing surface waves over the baffle. This kind of fluid flows should be analysed by a strongly dissipative hydrodynamic model.

## 2. Statement of the problem

### 2.1. Theory

Let a rigid circular base cylindrical tank of radius $R$ be partially filled by a fluid with a mean depth $h$. The inner periphery of the tank contains a thin rigid-ring plate (baffle), which divides the fluid height $h$ into $h_1$ and $h_2$. Here, $h_1$ is the mean height of the upper fluid layer (over baffle) and $h_2$ is the length between baffle and bottom. The thickness of the baffle is assumed to be negligible relative to $h_1$ and $h_2$. Furthermore, the fluid motions occurring due to initial perturbations are described within the framework of the inviscid incompressible hydrodynamic model with irrotational flows. In order to retain the baffle inside of the fluid bulk, the deflections of free-standing waves relative to hydrostatic equilibrium are assumed to be smaller than $h_1$.

The problem is studied in the scaled formulation suggesting that all the lengths and physical constants are normalised by $R$. This implies, in particular, that $h_1 := h_1/R$, $h_2 := h_2/R$, $g := g/R$ (the gravity acceleration $g$ has now the dimension $[s^{-2}]$) etc. The free-boundary problem is formulated in a tank-fixed coordinate system $Oxyz$. The $Oz$-axis is directed along the symmetry axis of the tank and the origin $O$ is posed on the baffle plane as shown for the hydrostatic state in Figure 1(a). Further, small initial perturbations

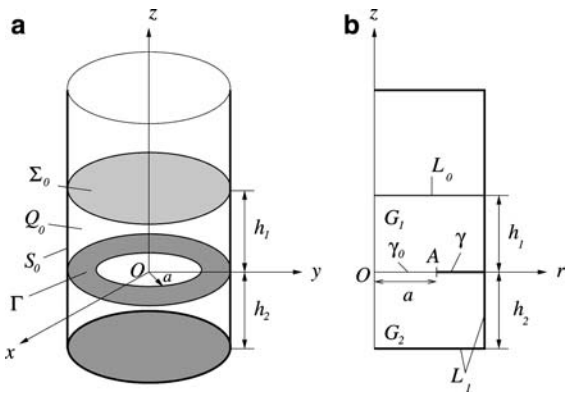


*Figure 1.* Hydrostatic fluid shape in a rigid cylindrical tank; three-dimensional and meridional sketches. The thin rigid-ring baffle $\Gamma$ is submerged into the fluid volume.

that initialise the linear free-standing gravity waves are assumed. Under certain circumstances, these waves can be found from the following problem [43,44]:

$$\Delta\tilde{\Phi}=0 \quad \text{in } Q_0; \quad \frac{\partial\tilde{\Phi}}{\partial\nu}=0 \quad \text{on } S_0 \text{ and } \Gamma; \quad \int_{\Sigma_0}\frac{\partial\tilde{\Phi}}{\partial z}\mathrm{d}S=0, \tag{1}$$

$$\frac{\partial\tilde{\Phi}}{\partial z}=\frac{\partial\tilde{f}}{\partial t}; \qquad \frac{\partial\tilde{\Phi}}{\partial t}+g\tilde{f}=0 \quad \text{on } \Sigma_0, \tag{2}$$

where $Q_0$ is the static fluid domain, $S_0$ is the statically wetted tank surface, $\Sigma_0$ coincides with the mean fluid surface, $\nu$ is the outward normal to $Q_0$, the function $\tilde{f}(x,y,t)$ defines small-amplitude elevations of the free surface ($z=\tilde{f}(x,y,t)$) and $\tilde{\Phi}(x,y,z,t)$ denotes the linear velocity potential. The boundary-value problem (1–2) is completed by the initial conditions

$$\tilde{f}(x,y,0)=\tilde{f}_0(x,y); \quad \frac{\partial\tilde{f}}{\partial t}(x,y,0)=\tilde{f}_1(x,y), \quad \int_{\Sigma_0}\tilde{f}_i\mathrm{d}S=0, \quad i=0,1, \tag{3}$$

where the prescribed functions $\tilde{f}_0$ and $\tilde{f}_1$ define initial fluid shapes and velocities of the free surface, respectively.

Solutions of the linear problem (1–2) are associated with a special class of spectral problems with a spectral parameter in the boundary conditions. Reduction to these spectral problems suggests the substitution

$$\tilde{\Phi}(x,y,z,t)=\varphi(x,y,z)\ \exp(\mathrm{i}\omega t), \quad \mathrm{i}^2=-1, \tag{4}$$

which defines natural frequencies $\omega$ and modes (complex amplitudes) $\varphi(x,y,z)$. By rewriting the boundary conditions (2) in the form

$$\frac{\partial^2\tilde{\Phi}}{\partial t^2}+g\frac{\partial\tilde{\Phi}}{\partial z}=0; \quad \tilde{f}=-\frac{1}{g}\frac{\partial\tilde{\Phi}}{\partial t} \quad \text{on } \Sigma_0 \tag{5}$$

and introducing $\kappa=\omega^2/g$, we may transform the evolutional problem (1), (5) to the spectral problem

$$\Delta\varphi=0 \quad \text{in } Q_0; \quad \frac{\partial\varphi}{\partial\nu}=0 \quad \text{on } S_0 \text{ and } \Gamma,$$
$$\frac{\partial\varphi}{\partial z}=\kappa\varphi \quad \text{on } \Sigma_0; \quad \int_{\Sigma_0}\varphi\mathrm{d}S=0. \tag{6}$$

As established by Eastham [45] and Feschenko *et al.* [43] for Lipschitzian domains $Q_0$ and by Gavrilyuk *et al.* [44] for non-Lipschitzian $Q_0$ (with baffles, for example), the spectral problem (6) has the real positive pointer spectrum $\{\kappa_i\}$, $\kappa_i \to +\infty$. Besides, $\{\varphi_i(x, y, h_1)\}$ constitute an orthogonal basis in $L_2(\Sigma_0)$ for any functions satisfying the integral condition of (6). These spectral theorems imply that eigenfunctions of (6) form, via formula (4), fundamental solutions of the evolutional problem (1–2): Knowing $\tilde{f}_0$ and $\tilde{f}_1$ in (3), we can find $\tilde{\Phi}$ by using the Fourier series in $\{\varphi_i(x, y, z)\}$ with time-dependent coefficients.

*Remark.* Although the functions $\varphi_i(x, y, h_1)$ are smooth and constitute an orthogonal basis in $L_2(\Sigma_0)$ [44], $\varphi_i(x, y, z)$ should belong to a suitable Besov space instead of the Sobolev space $H^1(Q_0)$. This is because $Q_0$ is not a Lipschitzian domain. Interested readers can find appropriate mathematical details in books by Kozlov *et al.* [46, Chapters 9–10], Lukovsky *et al.* [47, Sections 12–13] and, to some extent, in the paper by Gavrilyuk *et al.* [44].

### 2.2. Circular-base tanks with an annular baffle

The spectral problem (6) allows separation of the spatial variables in the $(r, \theta, z)$-cylindrical coordinate system ($x = r\cos\theta$, $y = r\sin\theta$, $z = z$). Introducing $\varphi(r, \theta, z) = \psi^{(m)}(z, r)\exp(\mathrm{i}m\theta)$, $m = 0, 1, \ldots$, we may reduce (6) to the $m$-parametric family of the following two-dimensional spectral problems in meridional cross-sections of $Q_0$:

$$
\begin{aligned}
&L_m(\psi^{(m)}) = \frac{\partial^2\psi^{(m)}}{\partial r^2} + \frac{1}{r}\frac{\partial\psi^{(m)}}{\partial r} + \frac{\partial^2\psi^{(m)}}{\partial z^2} - \frac{1}{r^2}m^2\psi^{(m)} = 0 \quad \text{in } G,\\
&\frac{\partial\psi^{(m)}}{\partial r} = 0 \quad \text{on } L_1; \quad \frac{\partial\psi^{(m)}}{\partial z} = 0 \quad \text{on } \gamma; \quad \psi^{(m)}(z, 0) < \infty,\\
&\frac{\partial\psi^{(m)}}{\partial z} = \kappa^{(m)}\psi^{(m)} \quad \text{on } L_0, \quad m = 0, 1, \ldots; \quad \int_{L_0} r\psi^{(0)}\mathrm{d}r = 0,
\end{aligned}
\tag{7}
$$

where geometric definitions of $G = G_1 \cup G_2$, $L_1$, $L_0$ and $\gamma$ are sketched in Figure 1(b).

A simple analysis shows that (7) has an analytical solution for either $a = 1$ (smooth circular-base tank without baffles) or $a = 0$ (horizontal baffle divides the tank into two non-connected volumes). The corresponding natural spectra $\kappa[h]_i^{(m)}$ and $\kappa[h_1]_i^{(m)}$, $i \geq 1$, can be written as follows:

$$
\kappa[h]_i^{(m)} = \alpha_{im}\tanh(\alpha_{im}h); \qquad \kappa[h_1]_i^{(m)} = \alpha_{im}\tanh(\alpha_{im}h_1),
\tag{8}
$$

where $\alpha_{im}$ is the $i$th root of the equation $J'_m(\alpha_{im}) = 0$ ($J_m(x)$ is the Bessel function of the first kind) and the corresponding eigenfunctions of (6) take the form

$$
\begin{aligned}
&\varphi[h]_i^{(m)} = J_m(\alpha_{im}r)\frac{\cosh(\alpha_{im}(z + h_2))}{\cosh(\alpha_{im}h)}\begin{cases}\cos m\theta,\\ \sin m\theta,\end{cases}\\
&\varphi[h_1]_i^{(m)} = J_m(\alpha_{im}r)\frac{\cosh(\alpha_{im}z)}{\cosh(\alpha_{im}h_1)}\begin{cases}\cos m\theta,\\ \sin m\theta,\end{cases}
\end{aligned}
\tag{9}
$$

respectively.

Spectral theorems reported by Gavrilyuk *et al.* [44] imply that $\kappa_i^{(m)}$ lie between $\kappa[h_1]_i^{(m)}$ and $\kappa[h]_i^{(m)}$, *i.e.*

$$
\kappa[h_1]_i^{(m)} \leq \kappa_i^{(m)} \leq \kappa[h]_i^{(m)}, \quad i = 1, 2, \ldots; \quad m = 0, 1, \ldots.
\tag{10}
$$

## 3. Approximate fundamental solutions

### 3.1. Reduction to integral equation

If $0 < a < 1$, the spectral problems (7) do not admit analytical solutions. Following Galitsin and Trotsenko [41] and Trotsenko [39,40], we consider an artificial $\gamma_0 = \{z = 0,\ 0 \leqslant r < a\}$ that extends $\gamma$ and cuts the original meridional domain $G$ into two rectangles $G_1$ and $G_2$ as shown in Figure 1(b). The original natural mode $\psi^{(m)}$ falls then into the following two functions defined in $G_1$ and $G_2$:

$$\psi^{(m)}(z,r) = \begin{cases} \psi^{(m,1)}(z,r), & (z,r) \in G_1, \\ \psi^{(m,2)}(z,r), & (z,r) \in G_2. \end{cases} \tag{11}$$

When considering the spectral problem (7), we see that these two function must satisfy

$$L_m(\psi^{(m,i)}) = 0 \quad \text{in } G_i, \quad \psi^{(m,i)}(z,0) < \infty, \quad i = 1,2 \tag{12}$$

and the boundary conditions

$$\begin{aligned} &\frac{\partial \psi^{(m,1)}}{\partial r} = 0 \quad (r = 1,\ 0 < z < h_1); \quad \frac{\partial \psi^{(m,1)}}{\partial z} = 0 \quad (z = 0,\ a < r < 1), \\ &\frac{\partial \psi^{(m,1)}}{\partial z} = \kappa^{(m)} \psi^{(m,1)} \quad (z = h_1,\ 0 < r < 1), \end{aligned} \tag{13}$$

for $\psi^{(m,1)}$,

$$\begin{aligned} &\frac{\partial \psi^{(m,2)}}{\partial r} = 0 \quad (r = 1,\ -h_2 < z < 0), \\ &\frac{\partial \psi^{(m,2)}}{\partial z} = 0 \quad (z = 0,\ a < r < 1), \\ &\frac{\partial \psi^{(m,2)}}{\partial z} = 0 \quad (z = -h_2,\ 0 < r < 1), \end{aligned} \tag{14}$$

for $\psi^{(m,2)}$.

In addition, since $\psi^{(m)}(r,z)$ and their first derivatives must be continuous at $\gamma_0$, Equations (12–14) must be accompanied by the following transmission conditions

$$\psi^{(m,1)}(0,r) = \psi^{(m,2)}(0,r) \quad (0 < r < a), \tag{15}$$

$$\frac{\partial \psi^{(m,1)}}{\partial z}(0,r) = \frac{\partial \psi^{(m,2)}}{\partial z}(0,r) = N_m^{\kappa^{(m)}}(r) \quad (0 < r < a), \tag{16}$$

where $N_m^{(\kappa^{(m)})}$ is an auxiliary function belonging, generally speaking, to the weighted space $H_\eta^{-1/2}(\gamma_0)$ $(\eta(r) = r)$. When $m = 0$, the integral condition of (7) leads to

$$\int_{L_0} r\psi^{(0,1)} \mathrm{d}r = 0 \quad \text{and} \quad \int_0^a r N_0^{\kappa^{(m)}}(r) \mathrm{d}r = 0.$$

The transmission procedure inputs a test value of $\kappa^{(m)} \notin \{\kappa[h_1]_i^{(m)},\ i = 1,2,\dots\}$ and assumes that $N_m^{\kappa^{(m)}}$ is already known. By combining conditions (13–16), we get the boundary-value problems (12)+(13)+(16) and (12)+(14)+(16). These have the following analytical Green functions

$$K_m^{(\kappa^{(m)})}(z,r;r_0)=\sum_{k=1}^{\infty}\frac{J_m(\alpha_{km}r)J_m(\alpha_{km}r_0)}{\alpha_{km}n_{km}^2\sinh(\alpha_{km}h_1-\vartheta_{km})}\cosh[\alpha_{km}(z-h_1)+\vartheta_{km}],$$
$$((r,z)\in G_1,\ \ r_0\in(0,a)); \tag{17}$$

$$K_m(z,r;r_0)=\sum_{k=1}^{\infty}\frac{J_m(\alpha_{km}r)J_m(\alpha_{km}r_0)}{\alpha_{km}n_{km}^2\sinh(\alpha_{km}h_2)}\cosh[\alpha_{km}(z+h_2)],$$
$$((r,z)\in G_2,\ \ r_0\in(0,a)), \tag{18}$$

where

$$\vartheta_{km}=\frac{1}{2}\log\left|\frac{\alpha_{km}+\kappa^{(m)}}{\alpha_{km}-\kappa^{(m)}}\right|,$$
$$n_{km}^2=\int_0^1 rJ_m^2(\alpha_{km}r)\mathrm{d}r=\frac{1}{2}\left(1-\frac{m^2}{\alpha_{km}^2}\right)J_m^2(\alpha_{km}).$$

These Green functions give rise to solutions in $G_1$ and $G_2$ as follows

$$\psi^{(m,1)}(z,r)=-\int_0^a N_m^{\kappa^{(m)}}(r_0)K_m^{(\kappa^{(m)})}(z,r;r_0)r_0\mathrm{d}r_0, \tag{19}$$

$$\psi^{(m,2)}(z,r)=\int_0^a N_m^{\kappa^{(m)}}(r_0)K_m(z,r;r_0)r_0\mathrm{d}r_0+\delta_{0m}C_0, \tag{20}$$

where $C_0$ is an arbitrary constant (henceforth, assumed to be equal to $-1$) and $\delta_{im}$ is the Kronecker delta implying $\delta_{0m}=0,\ m\neq 0;\ \ \delta_{00}=1$. The functions $\psi^{(m,1)}$ and $\psi^{(m,2)}$ must satisfy the transmission conditions (15). Inserting (19–20) into (15), we obtain the following integral equation

$$\int_0^a\left[K_m(0,r;r_0)+K_m^{(\kappa^{(m)})}(0,r;r_0)\right]N_m^{\kappa^{(m)}}(r_0)r_0\mathrm{d}r_0=\delta_{0m},\quad r\in(0,a), \tag{21}$$

with respect to $N_m^{\kappa^{(m)}}$ and $\kappa^{(m)}$.

Any solution of the spectral problem (7), that is a pair $(\kappa^{(m)},\psi^{(m)})$, determines a non-trivial solution $N_m^{\kappa^{(m)}}$ of (21). In turn, any non-trivial solution of (21) restores $\psi^{(m)}$ by Equations (19–20). One should note that, even if (21) has only numerical solutions (obtained, for instance, by a grid method), Equations (19–20) yield analytical approximate expressions for $\psi^{(m)}$.

*Remark.* If a test function $N_m^{\kappa^{(m)}}\in H_\eta^{-1/2}(\gamma_0)$, the integral of (21) generates an image $\tilde{N}_m^{\kappa^{(m)}}$ from $H_\eta^{1/2}(\gamma_0)$ and, therefore,

$$\left|\int_0^a rN_m^{\kappa^{(m)}}(r)\tilde{N}_m^{\kappa^{(m)}}(r)\mathrm{d}r\right|<\infty.$$

### 3.2. The Galerkin method

One way of solving the integral Equation (21) consists of using the Galerkin variational method. This suggests

$$N_m^{\kappa^{(m)}}(r)=\sum_{p=1}^{\infty}X_p^{(m,\kappa^{(m)})}f_p^{(m)}(r)\quad(0<r<a), \tag{22}$$

where $\{X_p^{(m,\kappa^{(m)})}\}$ are unknown and $\{f_p^{(m)}\}$ is an arbitrary family of complete functions from $H_\eta^{-1/2}(\gamma_0)$ (besides, the case $m=0$ requires $\int_0^a rf_p^{(0)}(r)\mathrm{d}r=0,\ \ p=1,2,\ldots$).

Substituting (22) in (21), accounting for the remark above and implementing the Galerkin projective procedure, we obtain the following infinite-dimensional system of linear homogeneous algebraic equations with respect to $X_p^{(m,\kappa^{(m)})}$

$$\lim_{p_0\to\infty}\sum_{p=1}^{p_0} X_p^{(m,\kappa^{(m)})} A_{pq}^{(\kappa^{(m)},m)} = 0, \quad (q = 1, 2, 3, \dots), \tag{23}$$

where

$$\begin{aligned} A_{pq}^{(\kappa^{(m)},m)} &= \sum_{k=1}^{\infty} B_{pk}^{(m)} B_{qk}^{(m)} \alpha_{km} n_{km}^2 \left[\coth(\alpha_{km}h_2) + \frac{\kappa^{(m)}\tanh(\alpha_{km}h_1) - \alpha_{km}}{\kappa^{(m)} - \alpha_{km}\tanh(\alpha_{km}h_1)}\right], \\ B_{pk}^{(m)} &= \frac{1}{\alpha_{km} n_{km}^2}\int_0^a f_p^{(m)}(r) J_m(\alpha_{km} r) r\,\mathrm{d}r. \end{aligned} \tag{24}$$

The linear system (23) has a non-trivial solution if and only if the test number $\kappa^{(m)}$ in (21) coincides with an eigenvalue from (7). After truncating (23), its necessary resolvability condition reads

$$\det\| \{A_{pq}^{(\kappa^{(m)},m)},\ \ p, q = 1, \dots, p_0\} \| = 0. \tag{25}$$

It can be considered as a transcendental equation with respect to $\kappa^{(m)}$. Computing roots of (25) yields approximate eigenvalues $\{\kappa_p^{(m)},\ \ p = 1, 2, \dots, p_0\}$. Non-trivial solutions $\{X_p^{(m,n)}\}$ of (23) make it possible to get approximate eigenfunctions.

The formulae given in the present paragraph are uniformly valid for any complete system of functions $\{f_p^{(m)}\}$.

Accuracy, convergence and numerical effectiveness of the Galerkin method can be improved with $\{f_p^{(m)}\}$, which have special asymptotic features at $r = 0$ and $r = a$. Studies by Keulegan and Carpenter [22] and Trotsenko [39] showed that

$$\frac{\partial\psi^{(m)}}{\partial z} \sim \sqrt{\frac{a}{2\pi}}\frac{1}{\sqrt{1-\left(\frac{r}{a}\right)^2}} \ \text{ as } r\to a; \quad \frac{\partial\psi^{(m)}}{\partial z} \sim r^m \ \text{ as } r\to 0. \tag{26}$$

The first limit of (26) shows that $N_m^{\kappa^{(m)}}(r) = \partial\psi^{(m)}/\partial z(r, 0)$ is singular at $r = a$. This singularity is caused by the vorticity stress at the baffle edge (interested readers are referred to thorough investigations of this stress as well as the related damping by Buzhinskii [25]).

### 3.3. Functional basis

The simplest example of functions $\{f_p^{(m)}\}$, which make it possible to satisfy (26) and, as a consequence, give adequate asymptotic prediction of $\psi^{(m)}$ at the point $A$ (see, Figure 1(b)) is

$$\begin{aligned} f_p^{(m)}(r) &= \frac{r^m}{\sqrt{1-\left(\frac{r}{a}\right)^2}}\left[1-\left(\frac{r}{a}\right)^2\right]^{p-1}, \quad (m, p = 1, 2, \dots), \\ f_p^{(0)}(r) &= f_p^{(*)}(r) - \frac{2p+1}{2p-1} f_{p+1}^{(*)}(r) \quad (m = 0;\ p = 1, 2, \dots), \end{aligned} \tag{27}$$

where

$$f_p^{(*)}(r) = \left[1-\left(\frac{r}{a}\right)^2\right]^{p-\frac{3}{2}}.$$

*Remark.* The quantities of the asymptotic expansions of $\psi^{(m)}(0,r)$ at $r=0$ and at the singular point $r=a$ (the latter can be obtained from results by Lukovsky *et al.* [47, Sections 12 and 13]) correspond to local quantities of (27). However, to the authors knowledge, the literature does not contain theorems on the completeness of $\{f_p^{(m)}\}$ in the weighted space $H_\eta^{-1/2}(0,a)$. This should give rise to special rigorous mathematical studies.

Substitution of (27) in the formulae of Section 3.2 gives analytical expressions for $B_{pk}^{(m)}$ and simplifies computations of the eigenfunctions (19–20). Derivations of these analytical expressions involve the integral presentation

$$J_{\mu+\nu+1}(z)=\frac{z^{\nu+1}}{2^\nu\Gamma(\nu+1)}\int_0^{\frac{\pi}{2}} J_\mu(z\sin\vartheta)\sin^{\mu+1}\vartheta\cos^{2\nu+1}\vartheta\,\mathrm{d}\vartheta,$$

with the gamma-function $\Gamma(x)$.

The coefficients $B_{pk}^{(m)}$ are

$$B_{pk}^{(m)}=\widetilde{b}_{pk}^{(m)}-\delta_{0m}\frac{2p+1}{2p-1}\widetilde{b}_{p+1,k}^{(m)},$$

$$\widetilde{b}_{pk}^{(m)}=\frac{a^{m+2}2^{p-\frac{3}{2}}\Gamma\left(p-\frac{1}{2}\right)J_{m+p-\frac{1}{2}}(\alpha_{km}a)}{\alpha_{km}n_{km}^2(\alpha_{km}a)^{p-\frac{1}{2}}},$$

and

$$\psi_n^{(m,1)}(z,r)=-\sum_{k=1}^{\infty}a_k^{(m,n)}J_m(\alpha_k r)g_k^{(m,n)}(r),$$

$$\psi_n^{(m,2)}(z,r)=\sum_{k=1}^{\infty}a_k^{(m,n)}J_m(\alpha_k r)g_k^{(m)}(r),\quad (m=0,1,2,\ldots),$$

where

$$a_k^{(m,n)}=\sum_{p=1}^{\infty}X_p^{(m,\kappa_n^{(m)})}B_{pk}^{(m)},$$

$$g_k^{(m,n)}=\frac{\cosh[\alpha_{km}(z-h_1)]}{\cosh(\alpha_{km}h_1)}\cdot\frac{\alpha_{km}+\kappa_n^{(m)}\tanh[\alpha_{km}(z-h_1)]}{\alpha_{km}\tanh(\alpha_{km}h_1)-\kappa_n^{(m)}},$$

$$g_k^{(m)}=\frac{\cosh[\alpha_{km}(z+h_2)]}{\sinh(\alpha_{km}h_2)}.$$

It should be noted that $A_{pq}^{(\kappa^{(m)},m)}$, $p,q=1,\ldots,p_0$ are determined by the series (24), which are functions of $\kappa^{(m)}$. This is why the accuracy in computing the roots of the transcendental equation (25) depends on the convergence of (24). Since

$$\alpha_{km}\approx k\pi;\quad J_m^2(\alpha_{km})\approx\frac{2}{\pi^2 k},\quad k\to\infty, \tag{28}$$

one can show that elements of (24) are

$$O\left(\frac{1}{k^{p+q}}\right),\quad m=0,1,2,\ldots;\quad p,q=1,2,\ldots,$$

and, therefore, the case $p=q=1$ is characterised by the weakest convergence. In order to improve this convergence, we should account for (28) and the fact that

$$S_m=\frac{2a^{2m+2}}{\pi}\sum_{k=1}^{\infty}\frac{\phi_k^{(m)}}{k^2},\quad \phi_k^{(m)}=\begin{cases}\sin^2 k\pi a, & (m=0,2),\\ \cos^2 k\pi a, & (m=1),\end{cases}$$

can be summed with the following result

$$S_m = \begin{cases} \pi a^{2m+3}(1-a), & (m=0,2), \\ \pi a^4\left(\frac{1}{3}+a^2-a\right), & (m=1). \end{cases}$$

This makes it possible to re-write (24) for $p=q=1$ in the form

$$A_{11}^{(\kappa,m)} = S_m + \sum_{k=1}^{\infty}\left\{(B_{1k}^{(m)})^2\alpha_{km}n_{km}^2[\coth(\alpha_{km}h_2)+\coth(\alpha_{km}h_1-\vartheta_k^{(m,n)})] - \frac{2a^{2m+2}\phi_k^{(m)}}{k^2\pi}\right\},$$

where the modified numerical series has the asymptotics $O(k^{-3})$ instead of $O(k^{-2})$.

For each fixed $m$, the basic system (27) includes only one singular function $f_0^{(m)}$, which implies local asymptotics (26) at the point $A$, but $f_p^{(m)} \in C[0,a]$, $p \geq 2$. Since $|f_0^{(m)}(r)| \to \infty$ and $|f_p^{(m)}| < \infty$, $p \geq 2$ as $r \to a$, the first basic function is in fact responsible for local flows in the neighbourhood of the baffle edge. When considering

$$\frac{\partial \psi^{(m)}}{\partial z}(0,r) = N_m^{\kappa^{(m)}} = X_0^{(m,\kappa^{(m)})} f_0^{(m)} + \tilde{N}_m^{\kappa^{(m)}},$$

$$\tilde{N}_m^{\kappa^{(m)}} = \sum_{p=2}^{p_0} X_p^{(m,\kappa^{(m)})} f_p^{(m)},$$

we obtain that a convergence study regarding the normal velocity on $\gamma_0$ and, therefore, to $\psi^{(m)}$ can be treated as

(i) convergence to the coefficient $X_0^{(m,\kappa^{(m)})}$ (local flows at $A$),

(ii) convergence to $\tilde{N}_m^{\kappa^{(m)}}$ in $C[0,a]$ (smooth component of the global flows associated with natural modes).

It should be noted, that $X_0^{(m,\kappa^{(m)})}$ determines the velocity intensity factor $K_v$ [25] and, therefore, accurate approximation of this coefficient allows for estimating the vorticity-based damping.

## 4. Numerical results and discussion

### 4.1. Convergence

Table 1 displays convincing and fast convergence to $\kappa_i^{(m)}$, $i=1,2,3,4$; $m=0,1,2$. The precision is high, even with a relatively small number of basic functions. Diverse numerical experiments with various $h_1$ and $a$ have shown that, if $h_1 \geq 0{\cdot}1$ and $a \geq 0{\cdot}3$, the numerical method always guarantees six significant figures of the lower eigenvalues $\kappa_1^{(m)}$, $m=0,1,2$ with the truncating dimension $p_0=5$.

A convergence analysis to $N_m^{\kappa^{(m)}}$ corresponding to $\kappa_1^{(m)}$, $m=0,1,2$ (and, as a consequence, to the eigenfunctions) shows that $p_0=7$ provides five significant figures of both $X_0^{(m,\kappa^{(m)})}$ (accuracy in approximating the local flows at $A$) and $\tilde{N}_m^{\kappa^{(m)}} \in C[0,a]$ (smooth component of the global flows). The same accuracy for some of the higher modes needed typically $p_0=8-9$. In these cases, the CPU time of our non-optimised FORTRAN codes (on a Pentium IV, 2·6 GHz computer) was about one second.

Approximate $\kappa_i^{(m)}$ are associated with roots of the transcendental Equation (25). Computing these needs iterative solvers, whose effectiveness and stability may depend on initial approximations of $\kappa_i^{(m)}$ (let us denote them $\tilde{\kappa}_i^{(m)}$). For $h_1 \geq 0{\cdot}1$, $a \geq 0{\cdot}3$, the numerical experiments showed that Newton's iterative method is stable for any $\tilde{\kappa}_i^{(m)}$ satisfying (10). However, the iterative computing becomes unstable for lower $h_1$ and $a$. In order to study the

influence of the initial approximations for $h_1 < 0{\cdot}1$, $a < 0{\cdot}3$, a path-following procedure with small stepping by $h_1$ and $a$ was employed. The procedure starts with roots of (25) computed (with a desired accuracy) for $h_1 = 0{\cdot}1$, $a = 0{\cdot}3$. Further, the truncating dimension $p_0$ has to be fixed and these roots should be used as $\tilde{\kappa}_i^{(m)}$ for lower $h_1$ and $a$. The procedure is repeated recursively. The numerical experiments showed that path-following is generally applicable to extend the numerical results to lower $h_1$ and $a$. However, it does not provide clear convergence to $\kappa_i^{(m)}$. The main reason is that the scheme is unstable for $p_0 > 8$. Secondly, the calculations exhibited strong sensitivity in stepping and broke down unconditionally for $h_1 < 0{\cdot}01$ and $a < 0{\cdot}1$. That is why, the present paper publishes results only for $h_1 \geq 0{\cdot}1$ and $a \geq 0{\cdot}3$.

The mentioned numerical instability for smaller $h_1$ can be explained from both mathematical and physical points of view. A mathematical explanation refers to the limiting spectral problem (7) with $h_1 = 0$ (the baffle lies on the unperturbed free surface). A detailed mathematical treatment of this problem (associated with sloshing in a hole) is given by Kuznetsov and Motygin [48]. Its solutions have logarithmic asymptotics at $r = a$ instead of (26). The

*Table 1.* Convergence to $\kappa_n^{(0)}, \kappa_n^{(1)}$ and $\kappa_n^{(2)}$, $n = 1, 2, 3, 4$ versus $p_0$ in (25) for $a = 0{\cdot}7$, $h_2 = 0{\cdot}5$ and two values of $h_1$ ($h_1 = 0{\cdot}1$ and $0{\cdot}5$).

| | | $h_1 = 0{\cdot}1$ | | | $h_1 = 0{\cdot}5$ | | |
|---|---|---|---|---|---|---|---|
| $n$ | $p_0$ | $\kappa_n^{(0)}$ | $\kappa_n^{(1)}$ | $\kappa_n^{(2)}$ | $\kappa_n^{(0)}$ | $\kappa_n^{(1)}$ | $\kappa_n^{(2)}$ |
| | 1 | 2·28607 | 0·93790 | 1·53476 | 3·75597 | 1·62183 | 2·90455 |
| | 2 | 2·28653 | 0·94024 | 1·53544 | 3·75910 | 1·62404 | 2·90621 |
| | 3 | 2·28654 | 0·94027 | 1·53544 | 3·75912 | 1·62404 | 2·90621 |
| 1 | 4 | 2·28655 | 0·94028 | 1·53544 | 3·75912 | 1·62404 | 2·90621 |
| | 5 | 2·28655 | 0·94028 | 1·53544 | 3·75912 | 1·62404 | 2·90621 |
| | 6 | 2·28655 | 0·94028 | 1·53544 | 3·75912 | 1·62404 | 2·90621 |
| | 7 | 2·28655 | 0·94028 | 1·53544 | 3·75912 | 1·62404 | 2·90621 |
| | 1 | 4·81039 | 2·98097 | 4·68493 | 7·00504 | 5·28665 | 6·69385 |
| | 2 | 6·12230 | 4·15960 | 5·88364 | 7·01042 | 5·31058 | 6·70035 |
| | 3 | 6·19683 | 4·18504 | 5·93413 | 7·01088 | 5·31187 | 6·70077 |
| 2 | 4 | 6·19733 | 4·18506 | 5·93441 | 7·01089 | 5·31188 | 6·70078 |
| | 5 | 6·19734 | 4·18506 | 5·93441 | 7·01089 | 5·31188 | 6·70078 |
| | 6 | 6·19734 | 4·18506 | 5·93441 | 7·01089 | 5·31188 | 6·70078 |
| | 7 | 6·19734 | 4·18506 | 5·93441 | 7·01089 | 5·31188 | 6·70078 |
| | 1 | 8·29360 | 6·26769 | 8·02229 | 10·17280 | 8·53331 | 9·96865 |
| | 2 | 8·55123 | 6·66552 | 8·39313 | 10·17294 | 8·53395 | 9·96887 |
| | 3 | 9·50380 | 7·82773 | 9·31368 | 10·17322 | 8·53525 | 9·96919 |
| 3 | 4 | 9·60561 | 7·92096 | 9·39597 | 10·17326 | 8·53539 | 9·96923 |
| | 5 | 9·60785 | 7·92226 | 9·39760 | 10·17326 | 8·53539 | 9·96923 |
| | 6 | 9·60788 | 7·92227 | 9·39761 | 10·17326 | 8·53539 | 9·96923 |
| | 7 | 9·60788 | 7·92227 | 9·39761 | 10·17326 | 8·53539 | 9·96923 |
| | 1 | 11·60040 | 9·68234 | 11·40933 | 13·32365 | 11·70581 | 13·17032 |
| | 2 | 11·86938 | 10·04555 | 11·66641 | 13·32365 | 11·70584 | 13·17033 |
| | 3 | 12·09188 | 10·29531 | 11·94871 | 13·32366 | 11·70588 | 13·17034 |
| 4 | 4 | 12·70927 | 11·05345 | 12·56100 | 13·32368 | 11·70594 | 13·17035 |
| | 5 | 12·80440 | 11·14807 | 12·64583 | 13·32368 | 11·70595 | 13·17036 |
| | 6 | 12·80820 | 11·15087 | 12·64899 | 13·32368 | 11·70595 | 13·17036 |
| | 7 | 12·80827 | 11·15091 | 12·64905 | 13·32368 | 11·70595 | 13·17036 |

alternative, namely physical treatment of the numerical failure should probably invoke the shallow-fluid analysis of the fluid layer over the rigid plate. By using the prediction of the shallow-like sloshing given by Faltinsen and Timokha [17], we observe that the case $h_1/(1-a) \lesssim 0{\cdot}2$ implies strongly nonlinear and dissipative flows [49, 50]. These can not be modelled by (1–2). The estimate $h_1/(1-a) \lesssim 0{\cdot}2$ is consistent with the inequalities $h_1 < 0{\cdot}1$ and $a < 0{\cdot}3$.

Even if $h_1$ is not small, the method can be invalid for small $a$ (annular baffle is relatively wide to prevent fluid flux between upper and lower fluid domains). The numerical failure is caused by the Green's function technique. The eigenvalues $\kappa_i^{(m)}$ are not only confined to (10), but also, due to spectral theorems by Gavrilyuk *et al.* [44], should monotonically vary with $a$ and

$$\kappa_i^{(m)} \to \kappa[h_1]_i^{(m)} + 0 \quad \text{as } a \to 0 \quad \text{and} \quad \kappa_i^{(m)} \to \kappa[h]_i^{(m)} - 0 \quad \text{as } a \to 1. \tag{29}$$

Physically, the first limit implies complete insulation of the upper fluid layers against inter-domain flows. The second limit corresponds to the smooth circular cylindrical tank without any baffles. Accounting for the first limit, one can see that, if a test value $\kappa^{(m)}$ approximates an eigenvalue with a small $a$, this approximation should be close to $\kappa[h_1]_i^{(m)}$, $i = 1, 2, \ldots$. The Green function (17) then becomes degenerate. The reason of the degenerating is the ill-possessedness of the boundary-value problem (12)+(13)+(16) and consequent division by zero in (17) when at least one root of (25) tends to an isolated $\kappa[h_1]_i^{(m)}$.

### 4.2. Surface-wave profiles determined by natural modes

The second equation of (5) makes it possible to define surface-wave profiles (natural surface modes) associated with eigenfunctions $\varphi$ as follows

$$z = F(r, \theta); \qquad F(r, \theta) = \kappa\varphi(r, \theta, h_1) = \frac{\partial\varphi}{\partial z}(r, \theta, h_1). \tag{30}$$

Physically, due to (4), these profiles determine the linear free-standing waves. Separating angular (in terms of $\theta$) and radial (along $r$) components and noting that the angular wave profiles are easily described by trigonometric functions, our analysis centres exclusively around the two-dimensional projections of $F(r, \theta)$ in the meridional cross-section, namely, around

$$z = F_i^{(m)}(r); \quad F_i^{(m)}(r) = \kappa_i^{(m)}\psi_i^{(m)}(h_1, r), \quad m = 0, \ldots; \quad i = 1, \ldots. \tag{31}$$

Examples of such radial profiles for $m = 0, 1, 2$; $i = 1, 2, 3$, are shown in Figure 2. The figure illustrates Bessel-like shapes for $a \to 1$ and $a \to 0$. The Bessel graphs $F_i^{(m)}(r) = J_m(\alpha_{im}r)$, $m = 0, 1, \ldots$; $i = 1, 2, \ldots$, are drawn by solid lines. Even if $0 < a < 1$, the natural surface modes maintain a Bessel-like behaviour. They have, in particular, the same number of local minima/maxima.

Quantitatively, deviations of $F_i^{(m)}(r)$ relative to $J_m(\alpha_{im}r)$ were calculated subject to the uniform norm

$$||F_i^{(m)} - J_m||_C = \max_{r\in[0,1]} |F_i^{(m)}(r) - J_m(\alpha_{im}r)|.$$

These deviations are larger for smaller $h_1$, but they become practically unimportant for $h_1 \geq 0{\cdot}3$ (do compare the first rows in Figures 2 and 3).

The next important point is that deviations of $F_1^{(m)}$, $m = 0, 1, 2$, are less than 1% for $0{\cdot}95 \leq a \leq 1$. This means that small baffles, which are more often used in applications, do not affect free-standing wave profiles, but, probably, only damping rates. The difference between $F_i^{(m)}(r)$ and $J_m(\alpha_{im}r)$ depends also on $m$ and $i$. After testing various $m, i, a$ and $h_1$, we found that the

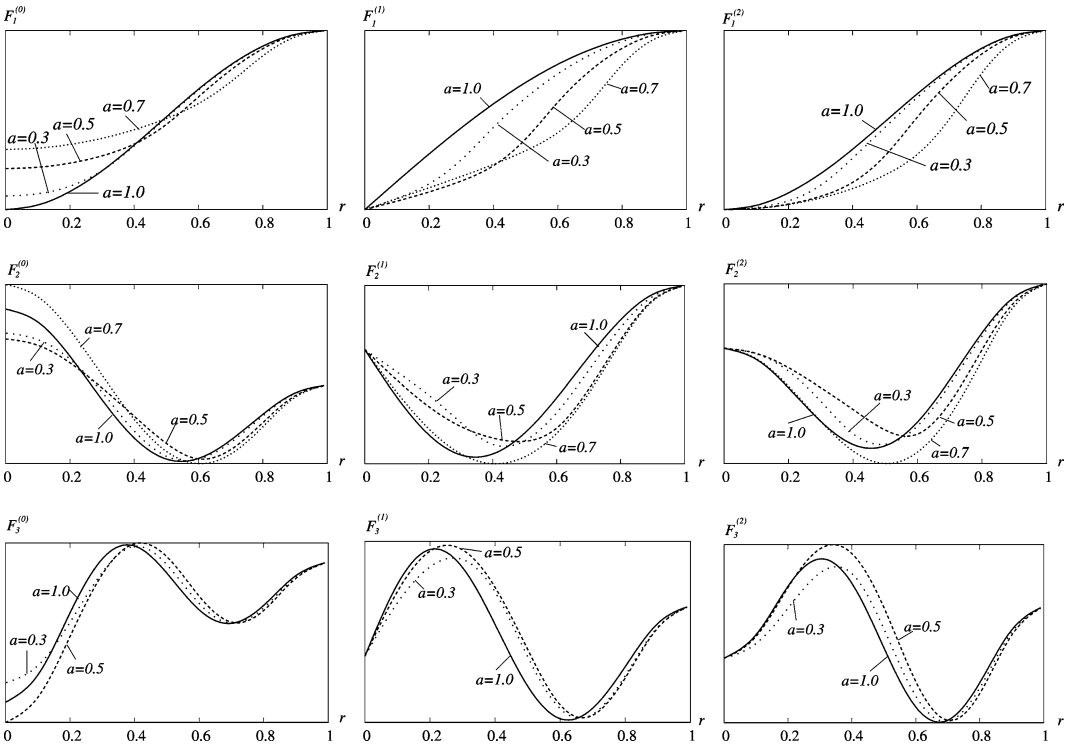


*Figure 2.* Meridional profiles of several lower natural modes for $h_1 = 0{\cdot}1$ and $h_1 + h_2 = 1$ versus $a$.

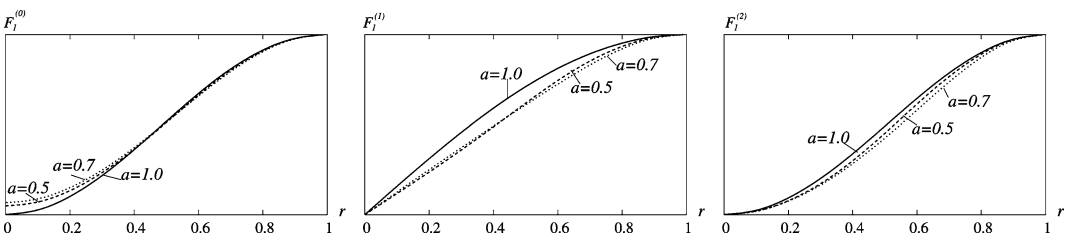


*Figure 3.* The same as in Figure 2, but with $h_1 = 0{\cdot}3$ and only for $F_1^{(m)}(r)$, $m = 0, 1, 2$.

difference is larger for $i = 1$. The maximum deviation between $F_1^{(m)}(r)$ and $J_m(\alpha_{1m} r)$ is established in the range $0{\cdot}54 < a < 0{\cdot}68$.

### 4.3. Natural frequencies versus $a$

Figure 4 illustrates typical monotonic dependences of $\kappa_i^{(m)}$ on $a$ (points on the left vertical border indicate the first theoretical limit of (29)). In order to quantify this theoretical monotonic dependence for diverse $h_1$ and $h_2$, various numerical experiments have been performed. These show that the graphs of $\kappa_i^{(m)}$ (as functions of $a$) are quite different for different $i, m$ and $h_1$. First of all, one should conclude that, if $h_1$ is relatively large ($h_1 > 0{\cdot}5$ in our numerical tests), the graphs imply practically a constant function, where $\kappa_i^{(m)}(a) \approx \kappa[h_1]_i^{(m)} \approx \kappa[h]_i^{(m)}$. Another important point is that the lower eigenvalues $\kappa_1^{(m)}, m = 0, 1, 2$, become very close to their lower limits $\kappa[h_1]_1^{(m)}$ as $a \leq 0{\cdot}5$ (see the first row in Figure 4). This means that $a \leq 0{\cdot}5$ yields the similarity problem – the fluid sloshing in a smooth vertical cylindrical tank with a fluid-filling level $h_1$ (or $a = 0$). In addition, we found that variations of $\kappa_1^{(m)}$, $m = 0, 1, 2$ are

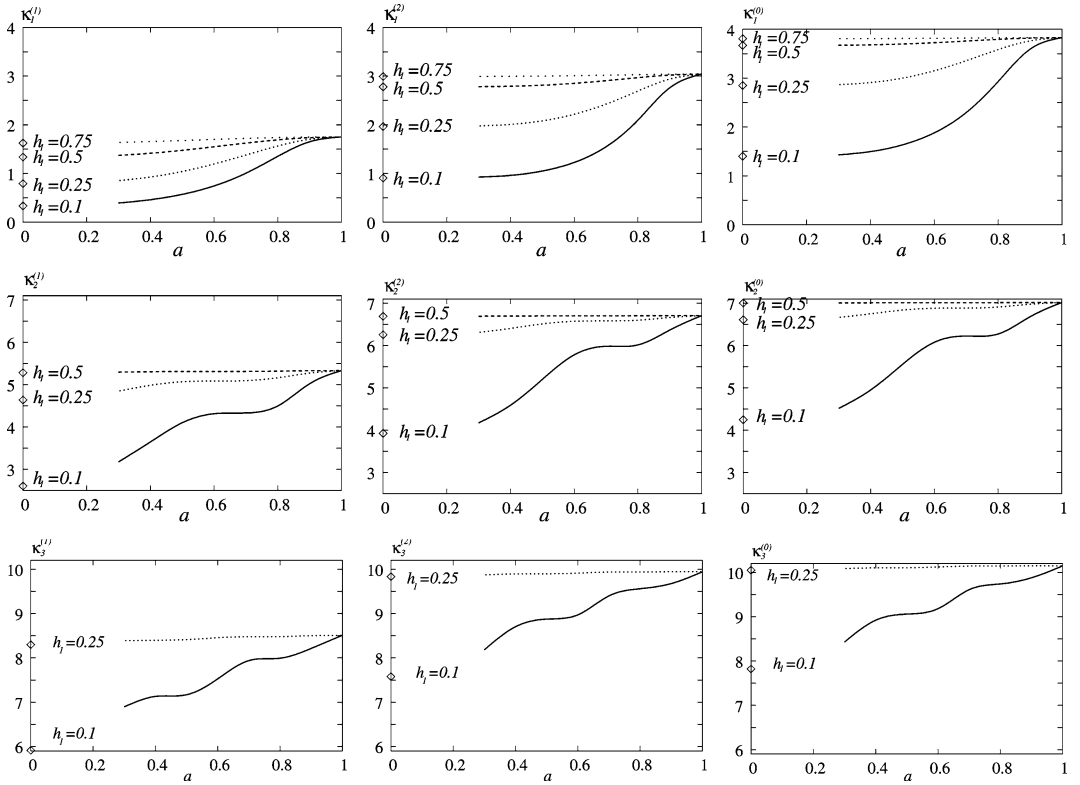


*Figure 4.* Eigenvalues $\kappa_i^{(m)}$, $m=0,1,2$; $i=1,2,3$ versus $a$ for $h_1+h_2=1$ and some isolated $h_1$.

less than 1% for $0{\cdot}95 \le a \le 1$. This implies that small baffles do not affect the lower natural frequencies.

We compared our numerical data with calculations by Müller [51] (for the first mode only) and the graphs by Gedikli and Ergüven [38] (corresponding to the first graph in Figure 4). These are in good agreement and, in particular, the difference from Müller is less than 2%.

Although quantification of higher frequencies is not as practically important as the lowest $\omega_{11}=\sqrt{g\kappa_1^{(1)}}$ (due to larger damping), we made some efforts to estimate some of the higher eigenvalues $\kappa_i^{(m)}$, $i \ge 2$ versus $a$. Examples are shown in the second and third rows of Figure 4. These demonstrate the inapplicability of the similarity problem above for higher natural frequencies and relatively small $h_1$ (equal to 0·1 in our calculations). The graphs in Figure 4 show also the quite different quantitative behaviour of $\kappa_i^{(m)}(a)$ with increasing integer parameter $i$, which is responsible for the wave steepness along the radial axis ($m$ implies the "angular" steepness). In spite of the monotonicity of all the graphs in Figure 4, the second derivatives $\partial^2\kappa_i^{(m)}/\partial a^2$, $i \ge 2$ change their signs at points $a_*$. The graphs of $\kappa_i^{(m)}(a)$ acquire a shelf-like shape in the neighbourhood of $a_*$. Our numerical analysis shows that the critical $a_*$ are close to the nodal points of $F_i^{(m)}(r)$, namely, $F_i^{(m)}(a_*) \approx 0$.

### 4.4. Natural frequencies versus $h_1$

Figure 5 illustrates qualitative theoretical results by Gavrilyuk *et al.* [44] on the monotonicity of $\kappa[h_1]_i^{(m)}$. As was been discussed in Section 4.3, the functions $\kappa[h_1]_i^{(m)} \approx \text{const}$, $i \ge 2$, for $h_1 > 0{\cdot}5$ (see the second and third rows in Figure 5). To find a physical explanation of this

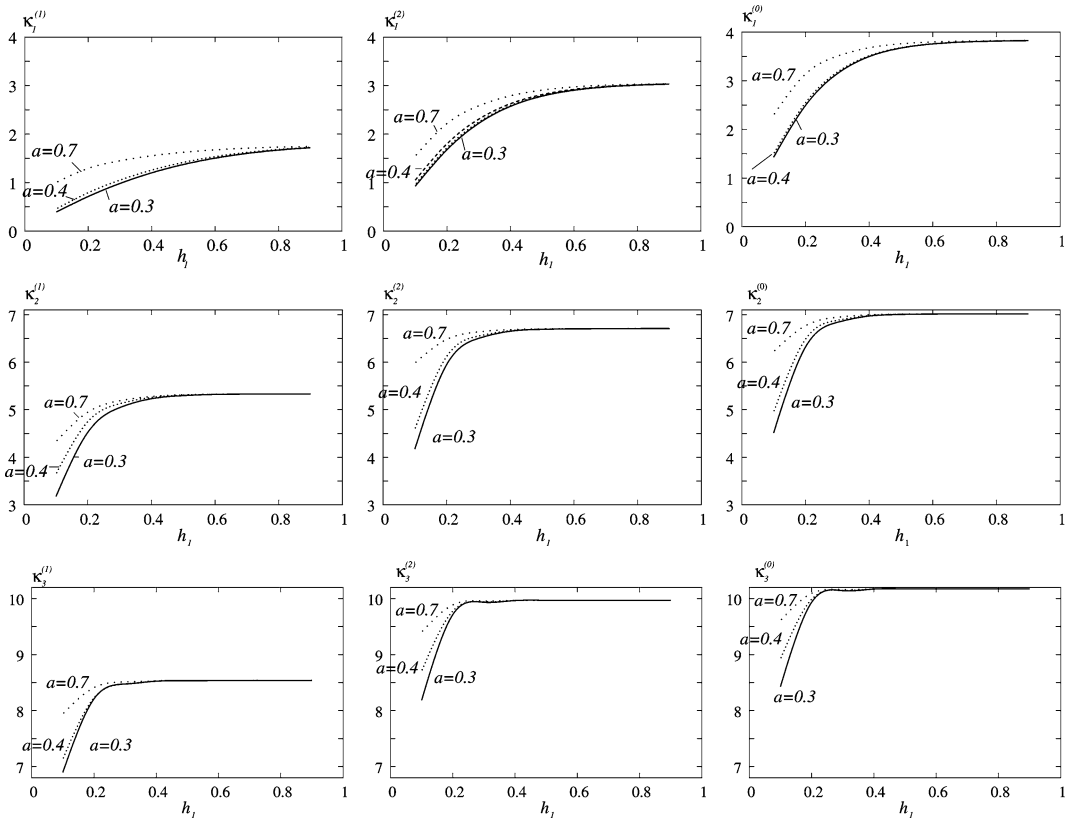


*Figure 5.* Eigenvalues $\kappa_i^{(m)}$, $m = 0, 1, 2$; $i = 1, 2, 3$ versus $h_1$ for $h_1 + h_2 = 1$ and some isolated $a$.

point, we point to the exponential decay, $\exp(\kappa_i^{(m)} z)$, of the natural modes $\psi^{(m)}(r, z)$ along the $Oz$-axis. From this viewpoint, $\kappa[h_1]_i^{(m)} \approx \text{const}$ may be true only for a few of the lower modes. This thesis is confirmed by the first row in Figure 5, which indicates a non-negligible difference between the graphs drawn for $a = 0{\cdot}3$ and $a = 0{\cdot}7$ (even in the range $0{\cdot}3 \leq h_1 \leq 0{\cdot}9$). Another very important theoretical conclusion by Gavrilyuk *et al.* [44] is that $\kappa_i^{(m)} \to 0$ as $h_1 \to 0$. We were not able to demonstrate this limit clearly, because of the numerical difficulties in handling small $h_1$ with the present Galerkin scheme (see discussion in Section 4.1).

## 5. Some concluding remarks

Pursuing an analytically oriented method to approximate the linear natural sloshing modes in tanks with baffles, we developed a robust, efficient, we believe, "elegant" numerical approach which captures the *analytical features of the velocity potential at the baffle edge*. It has a great many advantages relative to traditional numerical schemes that can be implemented to this linear fluid-sloshing problem. However, the method is less universal. It should be especially useful in debugging most general packages dealing with the fluid sloshing in tanks with baffles. Advantages and disadvantages of the analytical approximations in deriving nonlinear modal theories will be demonstrated in a forthcoming paper.

Another very important advantage of this method is the possibility of testing and analysing numerous positions and sizes of baffles within the tank and, therefore, of making the necessary physical and engineering conclusions. This has been demonstrated in the present

paper. The method can be extended to the linear sloshing problem involving circular cylindrical tanks with two and more annular horizontal baffles.

About limitations of the method the following can be said. These are found regarding the small distance allowed between the horizontal baffle and the hydrostatic fluid plane and the relatively width of the baffles (so that the baffle prevents flux between the upper and lower fluid volumes). This is a disadvantage from a theoretical, mathematical point of view, because we have initially expressed a desire to quantify several theoretical asymptotic limits on the natural frequencies represented by the theorems of Gavrilyuk *et al*. [44]. However, the untested limits, first of all for small $h_1$, are irrelevant. They are associated with shallow-fluid flows over the baffle and need other, dissipative and nonlinear physical models.

## Acknowledgements

This research has partially been sponsored by the German Research Council (DFG). A.T. acknowledges financial support of the Alexander von Humboldt Foundation.

## References

1. H.N. Abramson, *Slosh Suppression*. NASA Technical Report SP-8031 (1969) 467 pp.
2. H.F. Bauer, Zur Belastung, Trägheitsmoment Erhöhung und Schwappmassen Reduction durch Dämpfungsringe in Treibstofftank. *Raumfahrforschung* 4 (1967) 163–171.
3. G.I. Mikishev and B.I. Rabinovich, *Dynamics of Thin-Walled Constructions with Compartment Containing a Liquid*. Moscow: Mashinostroenie (1971) 563 pp. (in Russian).
4. G.I. Mikishev and G.A. Churilov, Some results on the experimental determining of the hydrodynamic coefficients for cylinder with ribs. In: I.B. Bogoryad (ed.), *Dynamics of Elastic and Rigid Bodies Interacting with a Liquid*. Tomsk: Tomsk university (1977) pp. 31–37 (in Russian).
5. G.I. Mikishev, *Experimental Methods in the Dynamics of Spacecraft*. Moscow: Mashinostroenie (1978) 247 pp. (in Russian).
6. R.A. Ibrahim, V.N. Pilipchuk and T. Ikeda, Recent advances in liquid sloshing dynamics. *Appl. Mech. Res.* 54 (2001) 133–199.
7. H.F. Bauer, Liquid sloshing in a cylindrical quarter tank. *AIAA J.* 1 (1963) 2601–2606.
8. H.F. Bauer, Liquid sloshing in $45^0$-compartmented sector tanks. *AIAA J.* 2 (1964) 768–770.
9. F. Solaas, *Analytical and Numerical Studies of Sloshing in Tanks*. Ph.D. thesis, Trondheim: Norwegian Institute of Science and Technology (1995) 268 pp..
10. A. Cariou and G. Casella, Liquid sloshing in ship tanks: a comparative study of numerical simulation. *Marine Structs.* 12 (1999) 183–198.
11. M. Arai, L.Y. Cheng and Y. Inoue, 3D numerical simulation of impact load due to liquid cargo sloshing. *J. Soc. Naval Archit. Japan* 171 (1992) 177–185.
12. M. Campolo, F. Sbrizzai and A. Soldati, Time-dependent flow structures and Lagrangian mixing in Rushton-impeller baffled-tank reactor. *Chem. Engng. Sci.* 58 (2003) 1615–1629.
13. S.M. Celebi and H. Akyildiz, Nonlinear modelling of liquid sloshing in a moving rectangular tank. *Ocean Engng.* 29 (2002) 1527–1553.
14. J.R. Cho and H.W. Lee, Dynamic analysis of baffled liquid-storage tanks by the structural-acoustic finite element formulation. *J. Sound Vibr.* 258 (2003) 847–866.
15. J.R. Cho and H.W. Lee, Numerical study on liquid sloshing in baffled tank by nonlinear finite element method. *Comp. Methods Appl. Mech. Engng.* 193 (2004) 2581–2598.
16. H. Ockendon, J.R. Ockendon and D.D. Waterhouse, Multi-mode resonance in fluids. *J. Fluid Mech.* 315 (1996) 317–344.
17. O.M. Faltinsen and A.N. Timokha, Asymptotic modal approximation of nonlinear resonant sloshing in a rectangular tank with small fluid depth. *J. Fluid Mech.* 470 (2002) 319–357.
18. S. Yalla, *Liquid Dampers for Mitigation of Structural Response: Theoretical Development and Experimental Validation*. Ph.D. Thesis, Notre Dame, Indiana: Department of Civil Engineering and Geological Sciences (2001) 346 pp.

19. O.M. Faltinsen, O.F. Rognebakke, I.A. Lukovsky and A.N. Timokha, Multidimensional modal analysis of nonlinear sloshing in a rectangular tank with finite water depth. *J. Fluid Mech.* 407 (2000) 201–234.
20. O.M. Faltinsen and A.N. Timokha, Adaptive multimodal approach to nonlinear sloshing in a rectangular rank. *J. Fluid Mech.* 432 (2001) 167–200.
21. T. Ikeda and N. Nakagawa, Non-linear vibrations of a structure caused by water sloshing in a rectangular tank. *J. Sound Vibr.* 201 (1997) 23–41.
22. G.H. Keulegan and L.H. Carpenter, Forces on cylinder and plates in a oscillating fluid. *J. Res. Natl. Bureau Stands.* 60 (1958) 423–440.
23. J.W. Miles, Ring damping of free surface oscillations in a circular tank. *J. Appl. Mech.* 25 (1958) 274-276.
24. T. Sarpkaya and J.L. O'Keefe, Oscillating flow about two and three-dimensional bilge keels. *J. Offshore Mech. Arctic Engng.* 118 (1996) 1–6.
25. V.A. Buzhinskii, Vortex damping of sloshing in tanks with baffles. *J. Appl. Math. Mech.* 62 (1998) 217–224.
26. M. Isaacson and S. Premasiri, Hydrodynamic damping due to baffles in a rectangular tank. *Canad. J. Civil Engng.* 28 (2001) 608–616.
27. I.A. Lukovsky, *Introduction to the Nonlinear Dynamics of a Limited Liquid Volume*. Kiev: Naukova Dumka (1990) 220 pp. (in Russian).
28. O.M. Faltinsen, O.F. Rognebakke and A.N. Timokha, Resonant three-dimensional nonlinear sloshing in a square base basin. *J. Fluid Mech.* 487 (2003) 1–42.
29. I. Gavrilyuk, I.A. Lukovsky and A.N. Timokha, A multimodal approach to nonlinear sloshing in a circular cylindrical tank. *Hybrid Methods Engng.* 2 (2000) 463–483.
30. L.V. Dokuchaev, On added inertia moment in a rotating cylinder with ribs. *Izvestiya AN USSR. Mech. Machinery* 2 (1964) 168–171 (in Russian).
31. B.I. Rabinovich, Effect of internal ribs on dynamic characteristics of a liquid in mobile containers. *Sov. Appl. Mech.* 6 # 8 (1970) 103–111 (in Russian).
32. V.I. Ermakov, G.A. Moiseyev and V.G. Shershnev, On perturbed motions of a body containing a cylindrical cavity with baffles. *Mech. Solids* 2 (1970) 52–61 (in Russian).
33. V.A. Trotsenko, Oscillations of a liquid in a circular cylinder with broken radial partitions. *Matematicheskaia Fizika* 9 (1971) 141–148 (in Russian).
34. V.N. Morozov, Application of a finite-difference method for solving the boundary value problems of the theory of perturbed motions of a rigid body with a fluid. In: V.G. Suvernev (ed.), *Oscillations of Elastic Structures with a Fluid*. Novosibirsk: Novosibirsk Energetic Institute (1974) pp. 161–165 (in Russian).
35. E.B.B. Watson and D.V. Evans, Resonant frequencies of a fluid container with internal bodies. *J. Engng. Math.* 25 (1991) 115–135.
36. K.S. Bisval, S.K. Bhattacharyya and P.K. Sinha, Free-vibration Analysis of liquid-filled tank with baffles. *J. Sound Vibr.* 259 (2003) 177–192.
37. A. Gedikli and M.E. Ergüven, Seismic analysis of a liquid storage tank with a baffle. *J. Sound Vibr.* 223 (1999) 141–155.
38. A. Gedikli and M.E. Ergüven, Evaluation of sloshing problem by variational boundary element method. *Engng. Anal. Boundary Elem.* 27 (2003) 935–943.
39. V.A. Trotsenko, Forced motions of a rigid carrier with an elastic annular plate. *Mech. Solids* 4 (1975) 78–88 (in Russian).
40. V.A. Trotsenko, Solutions of the boundary value problems associated with fluid dynamics in horizontal cylindrical cavities with partitions. *Nonlin. Oscill.* 6 (2003) 401–427.
41. D.A. Galitsin and V.A. Trotsenko, On determining the frequencies and added masses of a fluid in mobile cavities of rectangular parallelepipedal shape with partitions. *Mech. Solids* 2 (2001) 175–191 (in Russian).
42. R. Porter and D.V. Evans, Complementary approximations to wave scattering by vertical barriers. *J. Fluid Mech.* 294 (1995) 155–180.
43. S.F. Feschenko, I.A. Lukovsky, B.I. Rabinovich and L.V. Dokuchaev, *The Methods for Determining the Added Fluid Masses in Mobile Cavities*. Kiev: Naukova dumka (1969) 251 pp. (in Russian).
44. I.P. Gavrilyuk, A.V. Kulik and V.L. Makarov, Integral equations of the linear sloshing in an infinite chute and their discretisation. *Comp. Methods Appl. Math.* 1 (2001) 39–61.
45. M. Eastham, An eigenvalue problem with parameter in the boundary condition. *Q. J. Math.* 13 (1962) 304–320.
46. V.A. Kozlov, V.G. Maz'ya and J. Rossmann, *Elliptic Boundary Value Problems in Domains with Point Singularities*. Providence, RI: American Mathematical Society (1997) 414 pp.

47. I.A. Lukovsky, M.Ya. Barnyak and A.N. Komarenko, *Approximate Methods of Solving the Problems of the Dynamics of a Limited Liquid Volume*. Kiev: Naukova dumka (1984) 228 pp. (in Russian).
48. N. Kuznetsov and O. Motygin, Sloshing problem in a half-plane covered by a dock with two gaps: monotonicity and asymptotics of eigenvalues. *Comptes Rendus de l'Académie des Sciences, Series IIB, Mechanics* 329 (2001) 791–796.
49. W. Chester, Resonant oscillation of water waves. I. Theory. *Proc. R. Soc. London* 306 (1968) 5–22.
50. W. Chester and J.A. Bones, Resonant oscillation of water waves. II. Experiment. *Proc. R. Soc. London* 306 (1968) 23–30.
51. M. Müller, *Dreidimensionale Elastodynamische Analayse von Tanks mit Fluidbenetzten Einbauten*. Preprint TU-Branschweig, Series Mechanik (1993) N 8 46 pp.